Institute of Space and Aeronautical Science, University of Tokyo
Report No. 577, January 1980

SEPAC System Test in NASDA Space Chamber

By

Tatsuzo OBAYASHI, Kyoichi KURIKI, Nobuki KAWASHIMA,
Makoto NAGATOMO, Isao KUDO, Keiken NINOMIYA,
Akio USHIROKAWA, Masaki EJIRI and Susumu SASAKI

TABLE OF CONTENTS

1. INTRODUCTION

1.1 Purpose

This report reviews the test results of the second NASDA Space Chamber Test using SEPAC (Space Experiment with Particle Accelerators) proto-type models.

1.2 Scope

1) The second NASDA Space Chamber Test has been done with three main objectives which are

1. To determine safety level of electrical charge-up, i.e. correlation between

PFP (Floating Probe) data and spacecraft charge-up potential.
2. To evaluate EMI (Electromagnetic Interference) effect caused by electron beam and MPD (Magnetoplasmadynamic) arcjet firing.
3. To measure beam spread for EBA (Electron Beam Accelerator) software mask design.

The main part of this report is the results of the tests concerning these items.

2) In addition to them, the following two items are contained in this report.
1. To evaluate the capability of wire meshed beta cloth as return current collector.
2. To measure the effect of MPD firing on the surrounding equipment.

1.3 Test Configuration

The tests were carried out in two configurations:

1) Configuration I which uses accelerators and diagnostic probes operated by control and data management system.

2) Configuration II which uses accelerators and diagnostic probes operated by ground support equipments. Table 1 summarizes the instruments used in the experiment. The characteristics of each instrument are listed in Table 1–2.

TABLE 1–1. Summary of instruments used in 1978 NASDA experiment

	Configuration I	Configuration II
EBA		
EBA	PM	PM
GPS	PM	GSE
HVC	PM	GSE
MPD	PM	PM
PWR	PM	PM
DGP	EM	EM
MTV	EM and PM	EM and PM
CD		
IU	BBM	Controlled by GSE of each subsystem
DEP	PM	
CP	PM	
EMI Instruments	Antennae	Antennae
TRW	Faraday cup antenna	Faraday cup antenna
USU	Charge probe	Charge probe

TABLE 1-2. Characteristics of EBA, MPD and PWR

EBA (EBA and PWR, GPS and HVC)
- Electron gun with impregnated cathode
- Beam Energy : 0.1 ~ 7.5 keV
- Beam Current : 1.6 A Max.
- Perveance : 2.5×10^{-6} A/V$^{2.3}$
- Pulse width : Variable depending on Power

MPD (MPD, CAP and NGP)
- MPD arcjet plasma generator and NGP neutral gas plume generator
- MPD
  - Charging Voltage : 480 V
  - Energy : 2 kJ 3 atm.
  - FAV pressure : 3 atm.
  - FAV gas : Argon
  - Plasma : 10^{19} ion-electron pair/shot
  - Repetition : Every 15 seconds.
- NGP
  - GAS : N_2
  - Output gas/shot : 2.4/ NTP (Shuttle)
    20ccNTP (NASDA)

PWR (CHG and BAT)
- Charger for capacitor bank of MPD and Battery power supply for HVC
- Charger
  - Voltage : 500 V
  - Power : 1 kW max.
- BAT
  - Ni-Cd rechargable
  - Voltage : 480 V
  - Capacity : 4 AH

2. CHARGING BY THE ELECTRON BEAM EMISSION

The EBA subsystem is composed of EBA and HVC packages. In EBA package, an electron gun with deflection and focusing coils and power supplies for the electron gun (GPS) are assembled. The GPS has a capability to supply the cathode heater power, the beam current modulation pulse and the deflection and focusing coil power. The HVC can supply a high voltage power to the electron gun. Maximum beam energy and beam current are 7.5 keV and 1.6 A, respectively.

The proto-type model of EBA subsystem was used only in the configuration I. In the configuration II, only the electron gun was used and other components were replaced by ground support equipments.

The vacuum environment in the chamber was mostly kept at a pressure below 10^{-6} Torr so that the beam current of the designed value was extracted from the cathode all through the experiment. Fig. 2-1 shows the cathode activation characteristics and the process was followed as specified in the FO (Functional Objectives of the SEPAC SL-1 experiment). The voltage and current characteristic of the electron gun is shown in Fig.

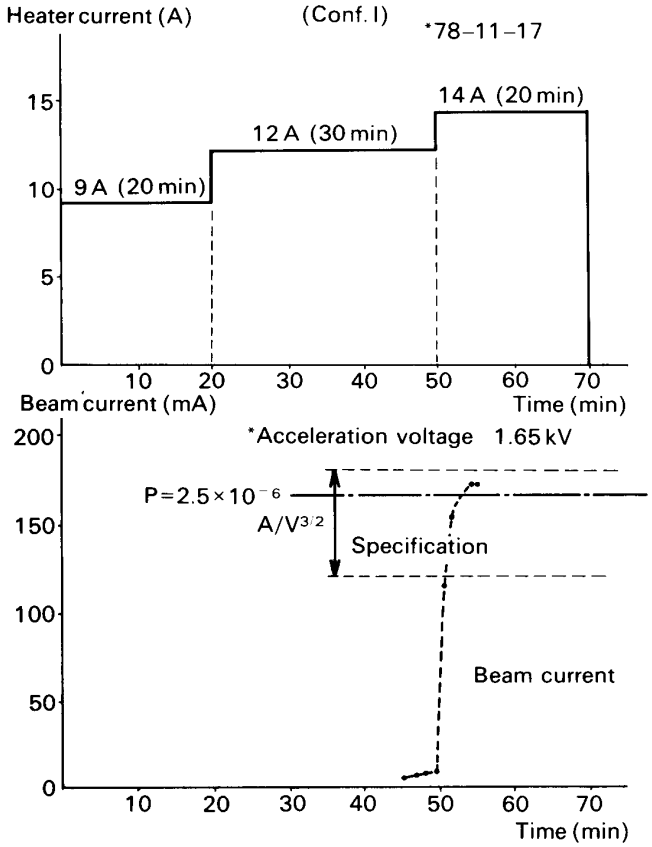

FIG. 2-1. Activation process of EBA.

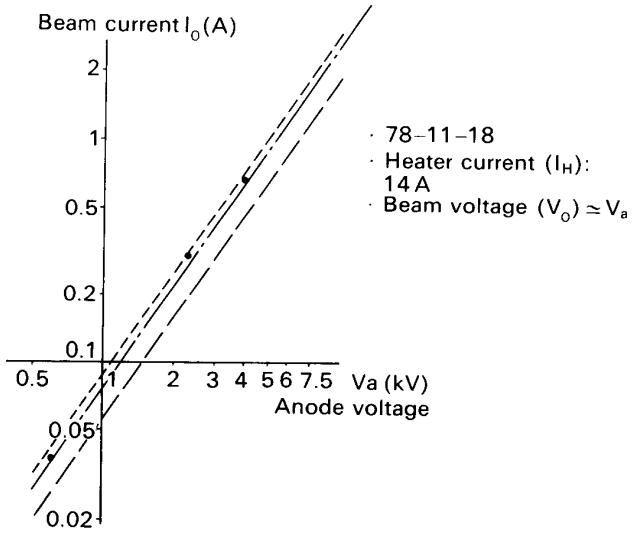

FIG. 2-2. Voltage-current characteristic of the activated electron gun.

2-2 and it agrees very well with the designed one (solid line). No degradation during the experiment was observed.

In the previous experiment that was done in 1977, an experiment was done to simulate the level I integration process at KSC. One of the electron guns used in that

experiment had been kept exposed to a dry air for a week before the experiment. No degradation was observed then. This time, the time period for the electron gun kept exposed to dry air was extended to 30 days. No noticeable effect of degradation was observed either.

2.1 Charging due to the Beam Emission

The floating mode experiment was done in the same configuration as the previous experiment in 1977. Not only all the components and the simulated pallet in the chamber but also the control and display devices outside the chamber were kept isolated from the chamber wall as shown in Fig. 2–3. The floating voltage as a function

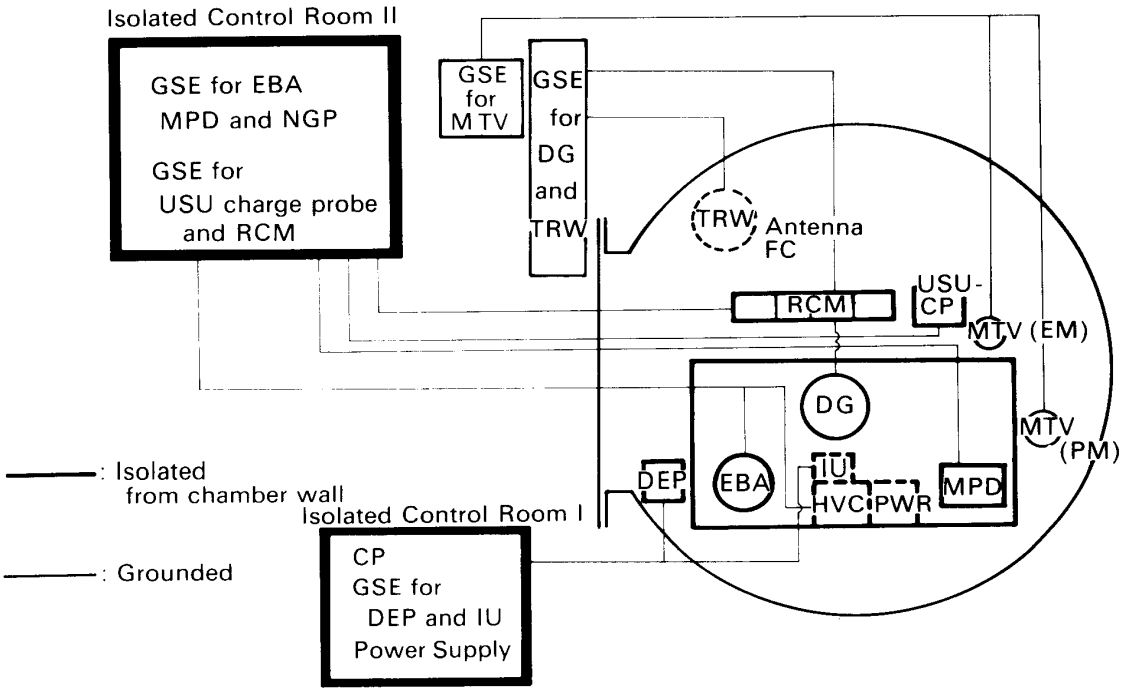

FIG. 2–3. Experimental layout.

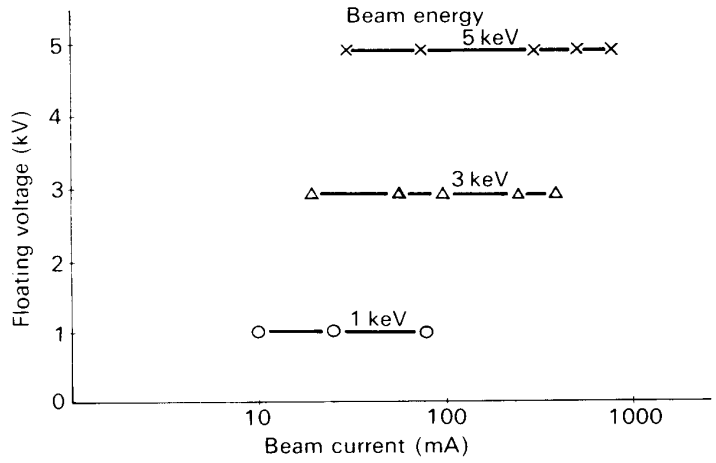

FIG. 2–4. Floating voltage of the pallet as a function of the beam current and energy.

of the beam voltage and current is shown in Fig. 2–4. The floating voltage was measured between the chamber wall and the system common directly by a high voltage probe. As is expected, the system was charged up completely to the voltage corresponding to the beam energy. When the system is charged up to the beam energy, the beam profile is not clear in the TV image. As will be shown later in Fig. 4–7 the system is vaguely bright, but beam trajectory is not clearly recognized. The system surface becomes bright due to the return current electron beam impingement.

2.2 *Charging Neutralization Experiment*

Charging Neutralization Experiments were done by using Neutral Gas Plume generator (NGP) and MPD arcjet.

2.2.1 *EBA-NGP Joint Experiment*

This time, the most of the gas in the NGP was ejected in one time by a mis-operation so that in the later experiment the amount of gas ejected was not enough. The background pressure rose only slightly so that the amount of gas ejected is estimated as about $2 \sim 3$ cc atm/shot. The time variation of the floating voltage due to the NGP activation is shown in Fig. 2–5. As seen from this figure, the floating voltage did not

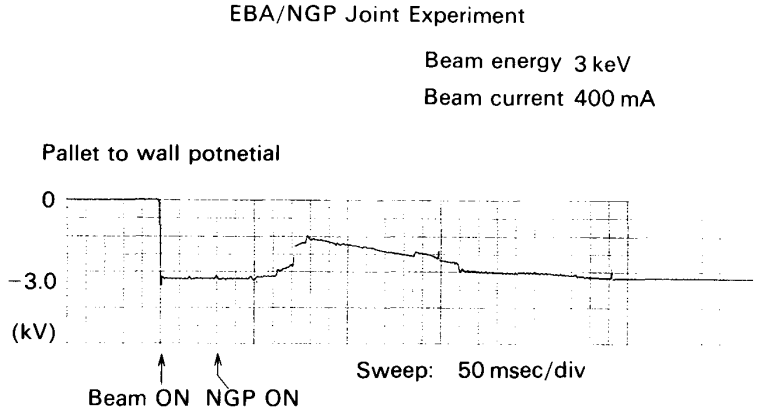

FIG. 2–5. Time variation of the pallet-to-wall potential in EBA/NGP experiment.

drop down to zero as in the previous experiment (Fig. 3.1.5 of ref. 1). Moreover, in the previous experiment, the effect of the neutral gas plume to neutralize the charging was more prominent for a larger beam current, but in this experiment, the neutral gas plume is more effective for a smaller beam current to neutralize the charging. When the neutral gas density is low in the neutral gas plume, the ionization by the beam electron is not in the discharge regime, or in other words, the number of electrons that can be produced by the beam electron is limited by the neutral gas density so that for a higher beam current, the number of beam ionized electrons per a beam electron decreases. It makes the drop of the floating potnetial smaller for a larger beam current. When the neutral density of the neutral gas plume had been large enough as in the previous experiment, the beam electron could have made a sufficient ionized electrons to produce a beam plasma discharge.

2.2.3 MPD-EBA Joint Experiment

The MPD-EBA joint experiment was done in such a way that first EBA was fired with a pulse width of about 5 sec and about one second after the rise of the beam current, the MPD arcjet was fired. A typical time variation of the floating voltage is shown in Fig. 2–6. The floating voltage drops at once when the MPD arcjet is fired and it persists for about 20–30 msec. This time period is determined by the decay of the plasma produced by the MPD arcjet in the chamber. As was discussed in the Ref. 1, this rather short time period in which the MPD arcjet is effective is due to the finite size of the vacuum chamber used in this experiment, though the chamber itself was a very large one.

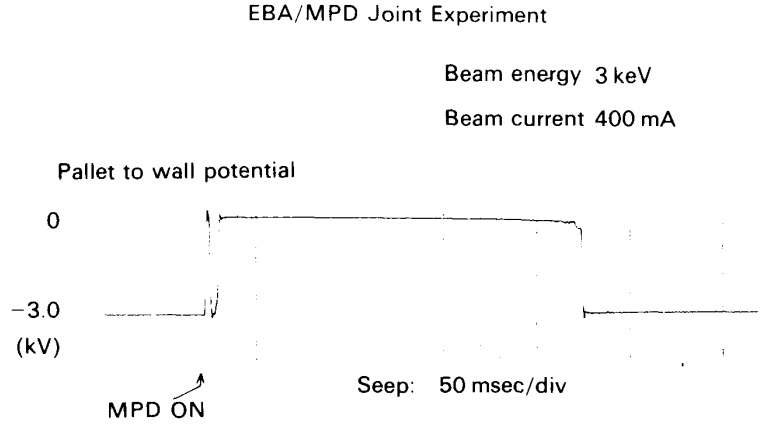

FIG. 2–6. Time variation of the pallet-to-wall potential in EBA/MPD experiment.

The floating potential once recovers but soon drops again, and this persists for very long period. In the MPD arcjet, a neutral gas is ejected from a puff before the discharge. After the discharge, however, still a considerable amount of neutral gas is coming out from the puff. It takes about 30 msec for the neutral gas to expands and fill the whole chamber. The background pressure rose to 10^{-5} Torr after the MPD was fired. This neutral gas cloud from the MPD arcjet contributes to neutralize the charging as a neutral gas plume.

2.3 Floating Probe Measurement

The floating probe (PLP-FP) used to detect a space potential relative to the pallet is composed of three electrodes (named as TOP, MID, and BOT respectively with each seperation distance of about 25 cm). The spatial potential distribution from the DGP (Diagnostic Package) surface to the finite distance is greatly dependent not only of the pallet potential itself, but also of the ambient space conductivity controlled mainly by the produced plasma density. This means the potential changes its spatial distribution with an experimental condition change even if the EBA firing condition is the same, namely the EBA alone, simultaneous firing with the MPD, or with the NGP (Neutral Gas Plume). Since the seperation distance of electrodes from the pallet is rather short compared to the system dimension and the pick-up resistance is finite, the detected potential does not always agree with the pallet potential. The laboratory experiment prior to in-flight measurement, however, gives a calibration of this PLP-FP data, that

is, a relation between a detected potential and the pallet potential.

Typical examples of obtained data with three different modes are illustrated in Fig. 2–7, 2–8, and 2–9 in which FE, EM, and EN are the modes of floating EBA, EBA with MPD and EBA with NGP respectively; AFT and PRE means after and prior (pre) to MPD or NGP firing. A pallet potential is a measure of the accelaration voltage of an electron beam, and in this experiment of floating mode it is demonstrated that the pallet potential is positively charged up to the voltage of an electron beam. A probe potnetial is usually negative to the pallet and the figures show a definite correlation with a pallet potential. The difference between AFT and PRE may be due to the difference of the surrounding environmental condition as mentioned above. The potentials detected by the TOP, MID and BOT probes range in this order of the probe array position from the pallet.

The measured floating voltage is much less than the floating voltage of the system. This is due to the fact that the thickness of the sheath around the system is very large so that all the floating probes are immersed in the sheath. The floating voltage was also measured by a charge probe brought from Utah State University, which is the proto-model of OFT-5 payload. The result will be reported elsewhere and it also shows a much less voltage than the actual floating voltage. Moreover, these charge probe and floating probes measurements strongly depend on the beam current. As can be seen in Fig. 2–4 and also in Fig. 3.1.3 (b) of Ref. 1 the actual floating voltage does not depend on the beam current when the beam current is above a certain value. This time all the experiment was done with a rather high beam current so that the floating voltage did

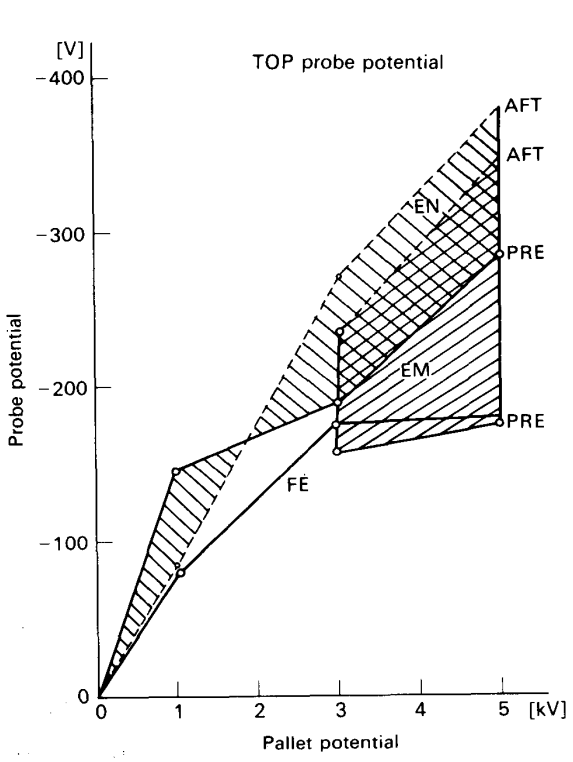

FIG. 2–7. Correlation between pallet and probe potentials.

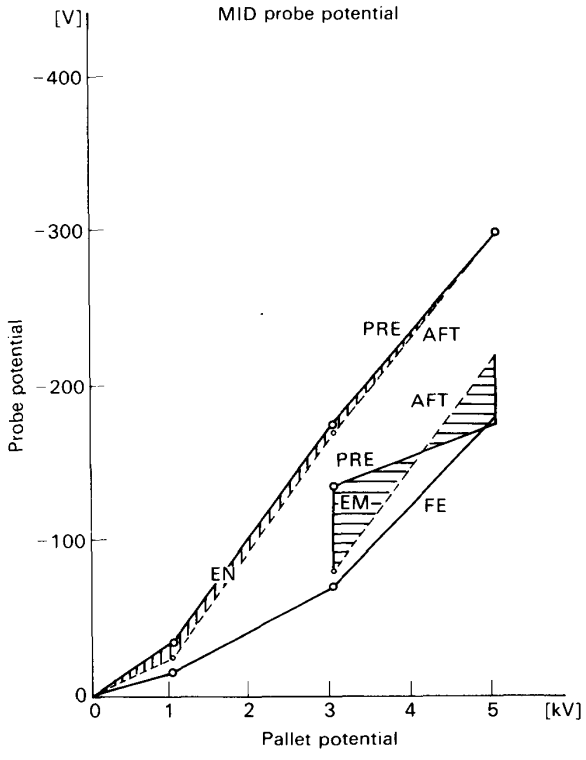

FIG. 2–8. Correlation between pallet and probe potentials.

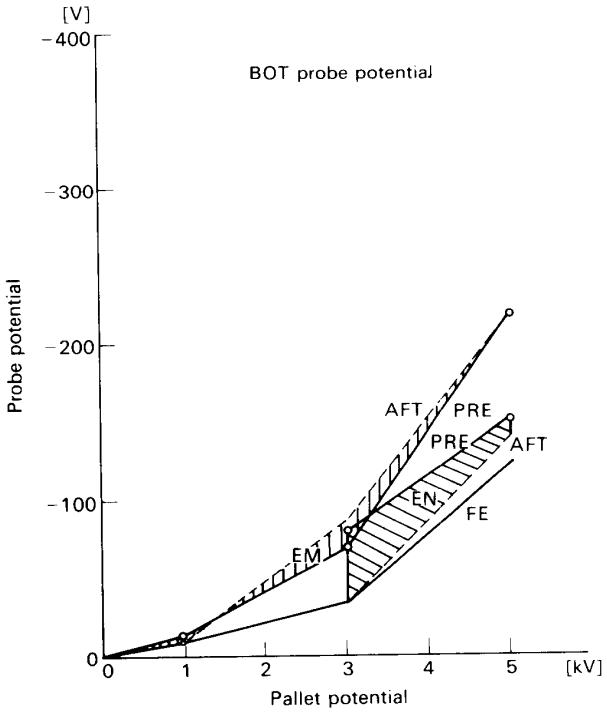

FIG. 2–9. Correlation between pallet and probe potentials.

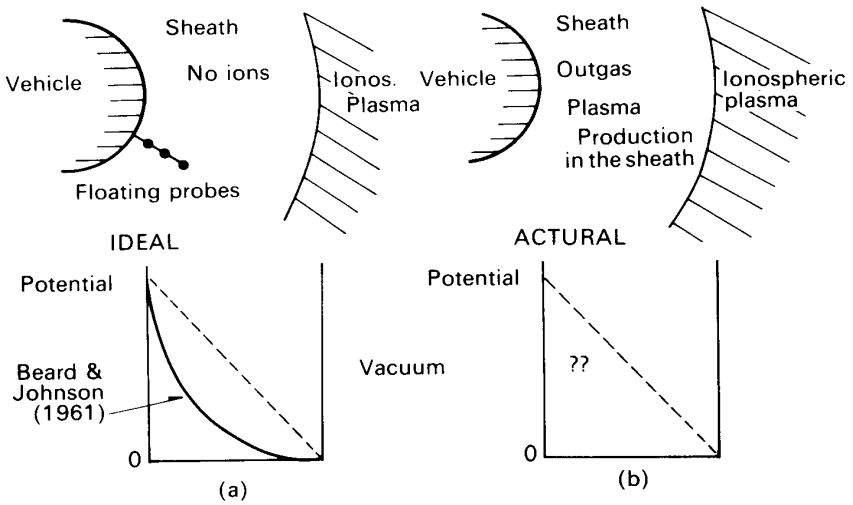

FIG. 2–10. Sheath formation around a charged in plasma.

not depend beam current and determined by only the beam energy. The reason why the signal from the charge probe and the floating probes depend on the beam current is explained as follows; When a conductive body is immersed in a plasma and set at a certain positive voltage, a sheath is formed around it and ions are expelled outside the sheath. In an ideal case, the potential distribution in the sheath is determined by Beard-Johnson model [2] and it is depicted schematically in Fig. 2–10 (a). Because the functional dependence of the potential distribution is known, it is easy to deduce the actual potential difference from the values which the floating probes measure even if they are immersed in the sheath.

The situation changes when plasma can be produced in the sheath. The positive

space charge in the sheath is neutralized by the produced plasma. The potential distribution becomes in general to the vacuum field which is loagrithmic in radius when the body is sphere (Fig. 2–10). Therefore it is very difficult to obtain the floating potential from the signals measured by those probes immersed in the sheath. The production of plasma in the sheath is not unusual in the beam experiment. Of course, when the neutral gas plume or the MPD arcjet plasma is used in the experiment, it is natural that the ionization occurs in the sheath. Even when no such neutralizing scheme is employed, a considerable amount of outgassing occurs on the surface near the electron gun due to the bombardment of returning electrons. This outgas cloud serves as a kind of neutral gas plume and the returning electrons as well as the primary electrons ionize the neutral gas cloud in the sheath.

In the laboratory experiment the floating potential can be measured directly as a potential difference between the chamber wall and the pallet by a high voltage probe, but in space experiment, it is impossible and the floating voltage should be determined from the measurement of those probes usually immersed in the sheath. The charging neutralization is clearly visualized in TV images taken by MTV. As already described, the trajectory is not clearly been seen when the system is charged up. When the MPD is fired and the charging is neutralized, the beam trajectory becomes very clear as will be shown later.

2.4 Wave Excitation by the Interaction of the Neutral Gas from the MPD Arcjet and the Electron Beam

As shown in Fig. 2–6, the floating voltage drops to zero due to the interaction of the

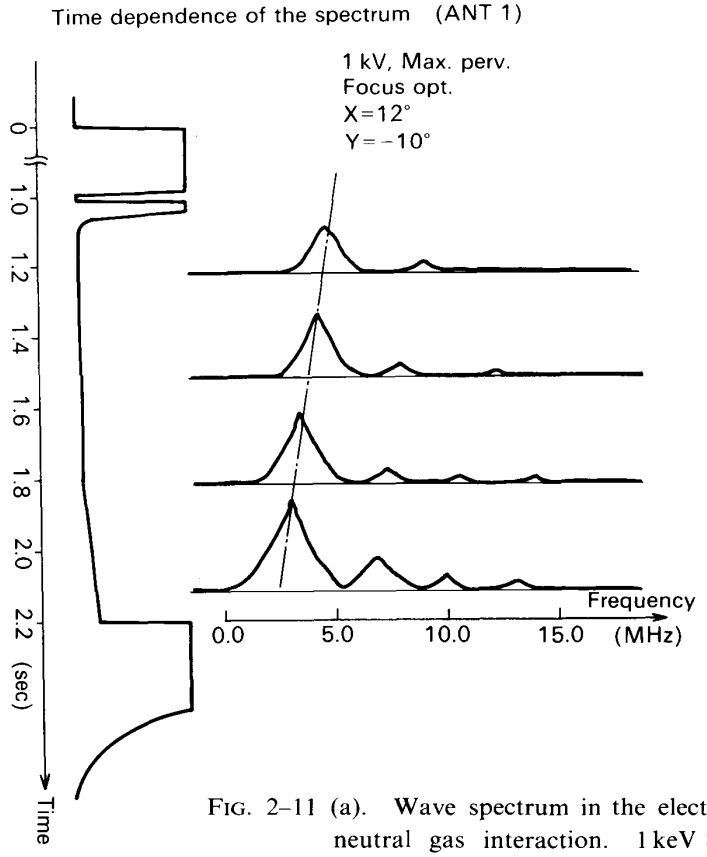

FIG. 2–11 (a). Wave spectrum in the electron beam-FAV neutral gas interaction. 1 keV 80 mA.

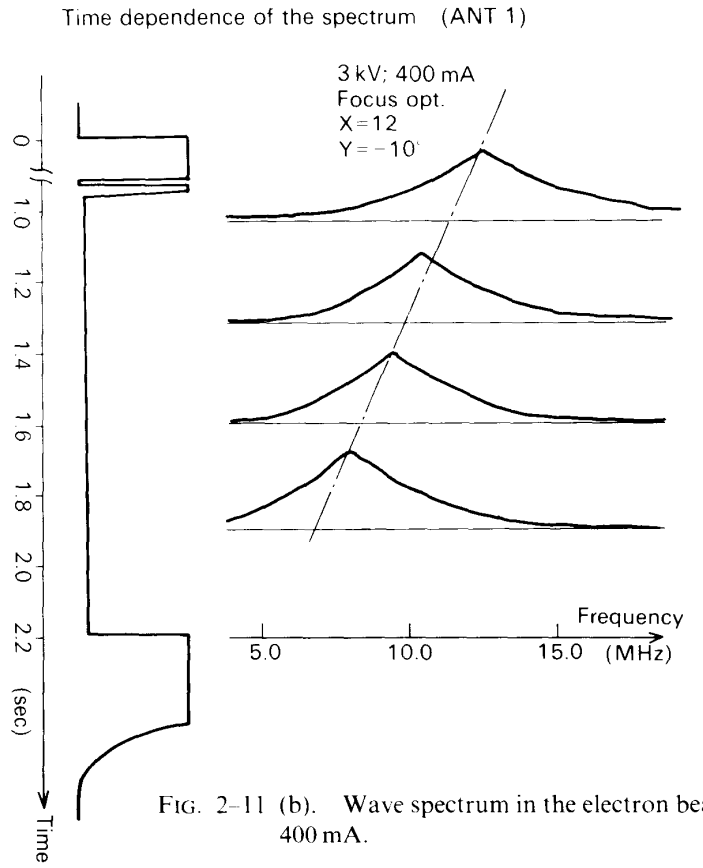

FIG. 2–11 (b). Wave spectrum in the electron beam-FAV neutral gas interaction. 3 keV 400 mA.

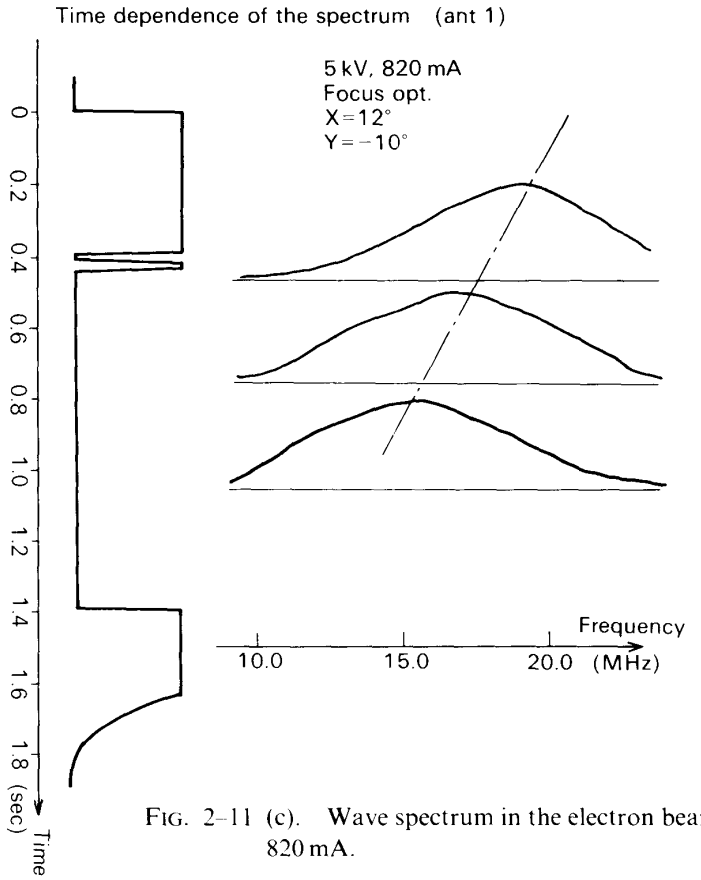

FIG. 2–11 (c). Wave spectrum in the electron beam-FAV neutral gas interaction. 5 keV 820 mA.

primary and returning electrons with the neutral gas cloud from the MPD arcjet. It is due to the plasma production by the interaction and the plasma neutralizes the charging. At the same time, the wave excitation was observed by a monopole antenna prepared by late J. M. Sellen of TRW. The location of TRW antennae was near the ceiling of the chamber. The signal was analysed by a spectrum analyser in the frequency range of 1 ~ 10 MHz and sweep rate was 3 Hz. As shown in Fig. 2–11 (a) ~ (c), the detected emission is observed only when the floating voltage drops due to the interaction of the beam and the neutral gas cloud. Its frequency decreases as the time goes on after the floating voltage drops. The emission may the upper hybrid resonance $\omega_{UHR}=\sqrt{\omega_{pe}{}^2+\omega_{ce}{}^2}$ where $\omega_{pe}=\sqrt{ne^2/m\varepsilon}$: electron plasma frequency and $\omega_{ce}=eB/m$: electron cyclotron frequency and in this case $\omega_{ce}/2\pi \approx 1$ MHz $\ll$ observed $\omega/2\pi$. The decrease of the frequency indicates that the neutral gas density gradually decreased because the gas is pumped out. The frequency becomes higher as the beam power is increased and it means that the plasma is produced more as the beam power is increased. The generation of harmonics is also observed and the spectrum becomes broad as the beam power is increased, indicating that a fairly strong non-linear interaction exists.

3. EMI Measurement Data

3.1 Test Objectives

Followings are the test objectives.

(1) Measurement of EMI level under MIL-STD-462

At previous NASDA chmaber test in 1977, almost all EMI data were above the specification [*1*]. Therefore, we must confirm at this time whether the electromagnetic noise is generated from SEPAC accelerator instruments or from the plasma beam itself. When we investigated previous chamber test results, amount of test cables inside the chamber were suspected to be prime sources of radiation.

Table 3–1. Test matrix

Mode	Measurement condition	Conducted emission					Radiated emission	
		Measurement items	01	02	03	04	02	04
Ambient	Dummy	HV Line (EBA)	×		×		×	×
		28V PWR Line	×		×			
EBA	Dummy	HV Line	×		×		×	×
	Beam ejection	HV Line	×		×		×	×
MPD	Dummy	28V PWR Line	×		×		×	×
	Beam ejection	28V PWR Line	×		×		×	×
EBA-MPD	Dummy						NA	NA
	Beam ejection						×	×

(2) Comparison of EMI level between dummy load mode and beam firing mode. It is based on the recommendation at 5th SEPAC meeting held at MSFC last Feb.

(3) Precise measurement at orbiter's critical frequencies and investigation on electromagnetic disturbance on the orbiter's communication system.

(4) Verify compatibility of DEP and IU for SEPAC accelerator subsystem under plasma emvironment.

3.2 Test matrix

Test matrix shown in Table 3–1. Test procedures are followed by previous test ones [*1*]. At this test, radiated emission measurement is the most important item and conducted emission measurement was minimized. Tests were made at Configuration I and II. Most data were taken at Configuration II. There, HVC (High Voltage Converter) and GPS (Gun Power Supply) were not used, owing to a failure happened during thermal vacuum test. Therefore, external power supplies were used.

3.3 Antenna and Probe Locations

Location of rod antennas and that of horn, conical, biconical and loop antennas are shown in Fig. 3–1 and Fig. 3–2. Current probes were set at 28V PWR line and high voltage line from HVC Simulater to EBA Head.

3.4 Frequency Characteristics of SEPAC Instruments

Frequency matrix is shown in Fig. 3–3 and it's identification is shown in Table 3–2. Frequencies are mostly generated at DC-DC converters. Rectangular shape wave forms were used except that HVC used sinusoidal one. In case of CHG (Charger), five frequencies are selected for different load power level. In HVC, generated frequency

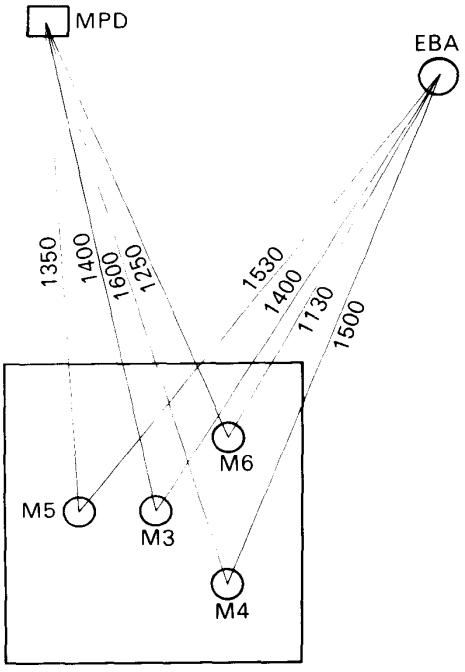

FIG. 3-1. Location of rod antennas.

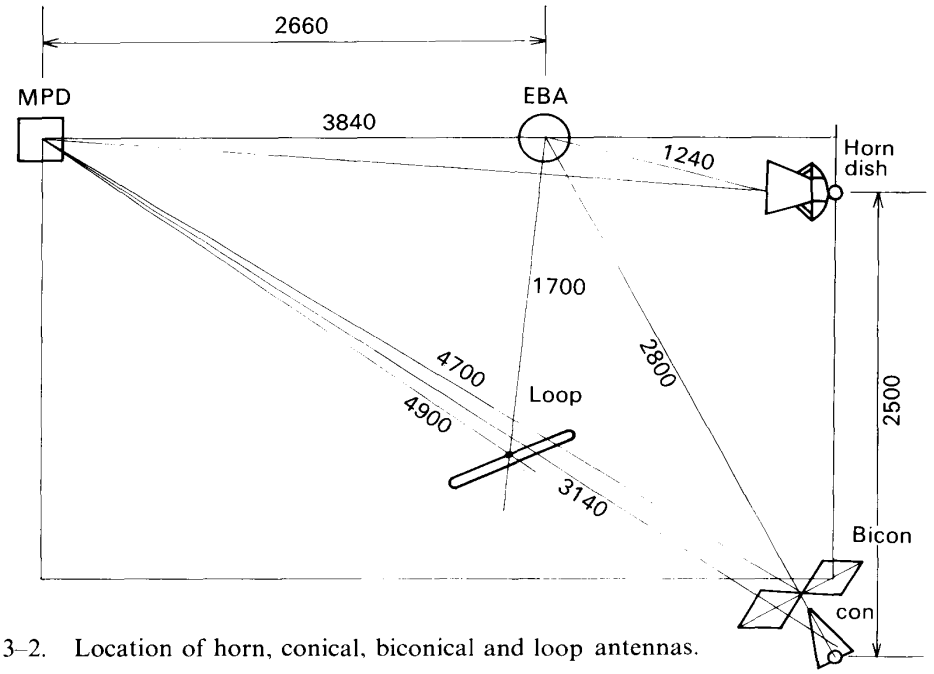

FIG. 3–2. Location of horn, conical, biconical and loop antennas.

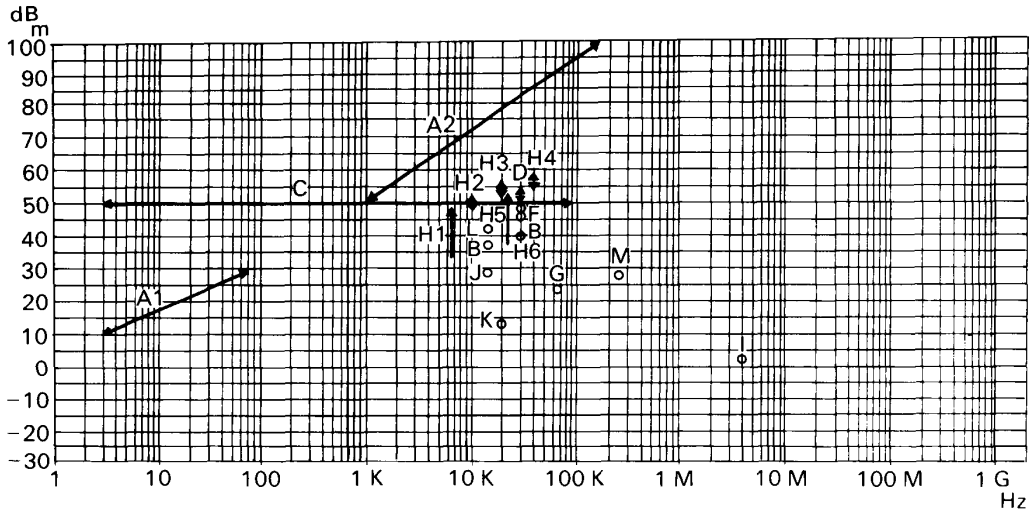

FIG. 3–3. Frequency matrix.

varies from 3 Hz to 150 kHz in order to cover wide range of operation. Other converters are operated at fixed frequencies.

3.5 Test Results and Discussions

(1) EBA RE (Electric Field)

Powers were fed from outside the chamber and high voltage power level was selected relatively moderate value of −5 kV, 660 mA against max. value at space experiment of −7.5 kV, 1.6 A. In Fig. 3–4, RE Radiated Emission measurement data for EBA dummy is shown. All points are controlled. Data for EBA firing are shown in Fig. 3–5. These results are extremely different from those obtained at previous test. At that time,

TABLE 3-2. Frequency identification

No.	Copm.	Unit	Freq. (Hz)	Remarks
A1	HVC	Main converter	Variable	No Load cond.
A2		Main converter	Variable	Load cond.
B	Batout SW trig	15 K		
C		HVC Trig	Variable	
D	GPS	Heater converter	30 K	
E		Anode converter	30 K	
F		Aux. converter	30 K	
G	MPD	IU Converter	66 K	
H1	PWR	CHG Converter	6.6 K	0-75 W for cap CHG
H2			10.1 K	75 W-140 W
H3			22 K	140 W-275 W
H4			40 K	285 W-600 W
H5			22 K	0-120 W for bat CHG
H6		Aux. converter	30 K	
I	MTV	Sync.	4.0 M	
J		Blanking	15.7 K	
K		HV Converter	20 K	
L	DGP	EPA-V Converter	15 K	
M		PHO Converter	250 K	

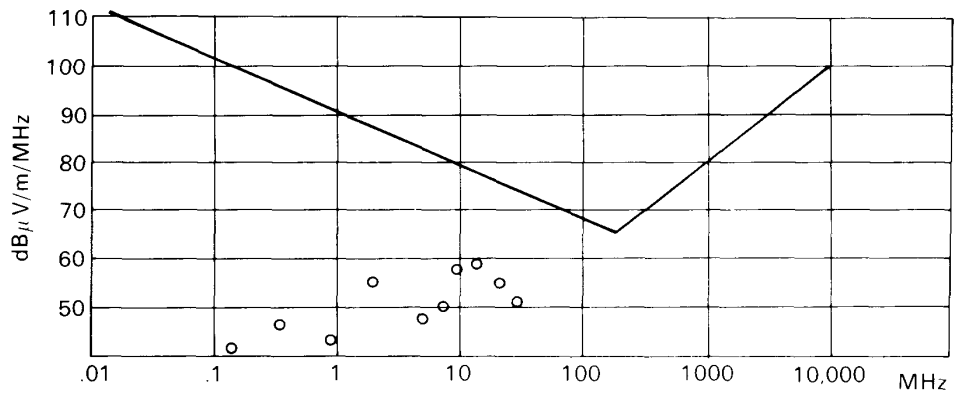

FIG. 3-4. EBA RE02 (BB) Dummy 5 kV.

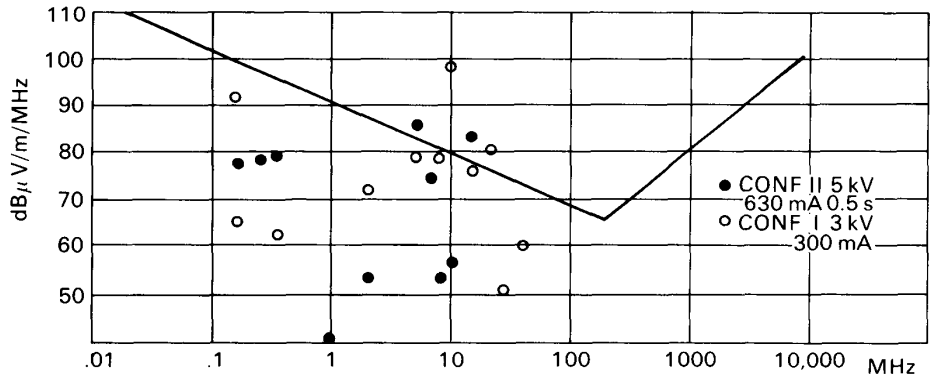

FIG. 3–5. EBA RE02 (BB) Fire.

enormous radiation was observed. Previous system was completely floated and electrical discharge at franges might have caused high EMI level. At this time, system was set at ground mode and HVC and GPS-high power noise devices were not used. It is shown that there is no remarkable noise above 30 MHz. Data obtained at Configuration I are also shown. We must note that power level was only 1 kW though HVC and GPS were included. At Configuration I, triggering signal for measurement instruments was not provided. Therefore, we did not have enough data.

(2) MPD RE (Electric Field)

Data obtained at MPD dummy load mode are shown in Fig. 3–6. All points are

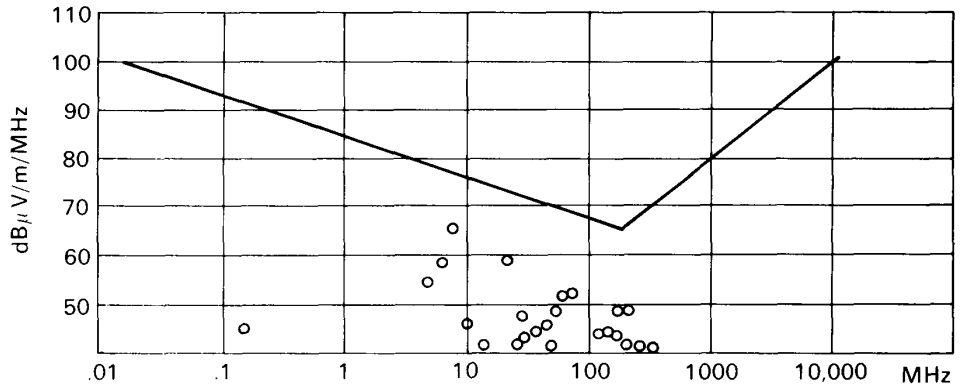

FIG. 3–6. MPD RE02 (BB) Dummy 480 V.

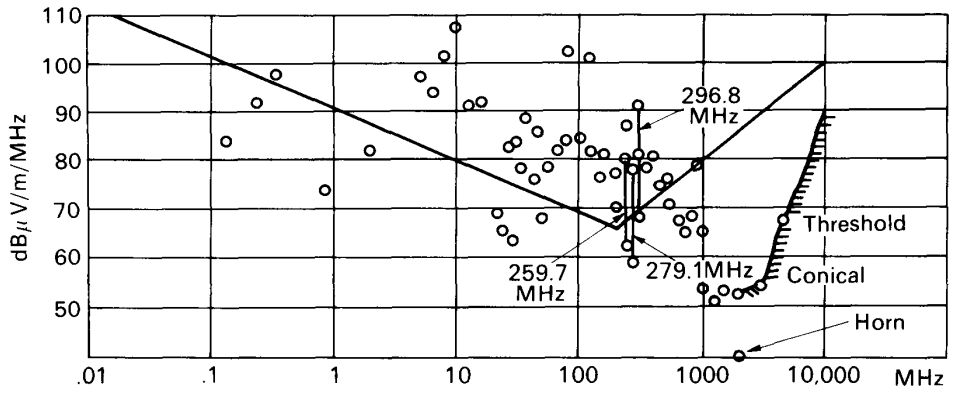

FIG. 3–7. MPD RE02 (BB) Fire 480 V 3 ATM.

below the specification. But when MPD is firing, data are widely scattered as shown in Fig. 3–7. Strong noise during MPD firing may result from electrical discharge at plasma sheath inside MPD Head. It is difficult to distinguish plasma frequency inside the Head and it is considered to distribute over wide frequency range. Noise from plasma column itself may be milder, since noise level above 1 GHz is small. Configuration of the data points obtained at this time are simillar to that obtained at previous test, but 30 dB noise reduction was achieved. Noise from plasma beam is regarded as intentional one and can be exempted from obeying the EMI specification. We can not control plasma beam itself. But we will be still required to reduce noise as much as possible, even if above description is true.

(3) EBA CE (Power Line)

High voltage line was selected as an important CE (Conducted Emission) measurement item. Data for dummy mode and firing mode are shown in Fig. 3–8 and

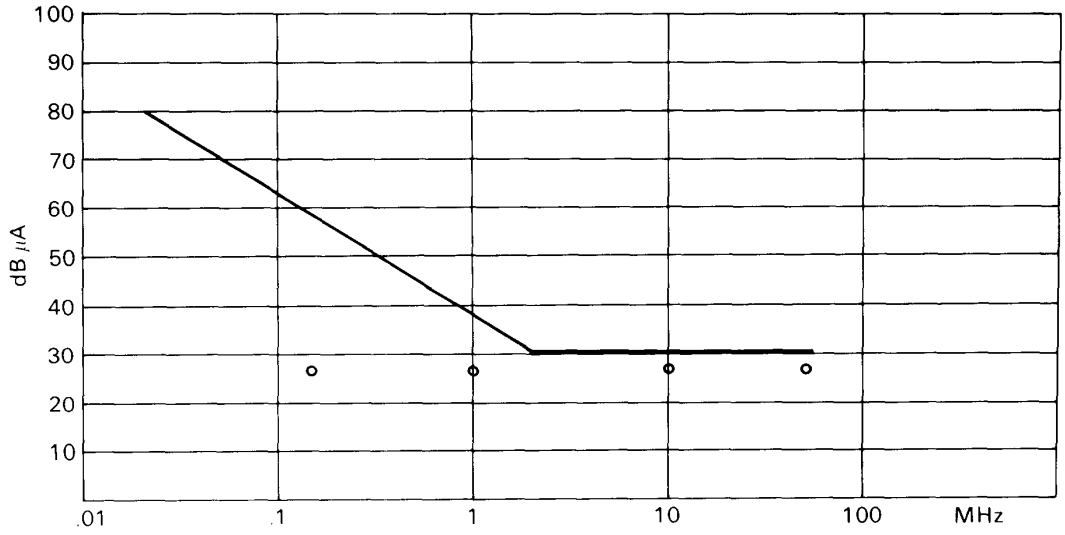

FIG. 3–8. EBA CE03 DH (NB) Dummy 5 kV 630 mA 0.5 s.

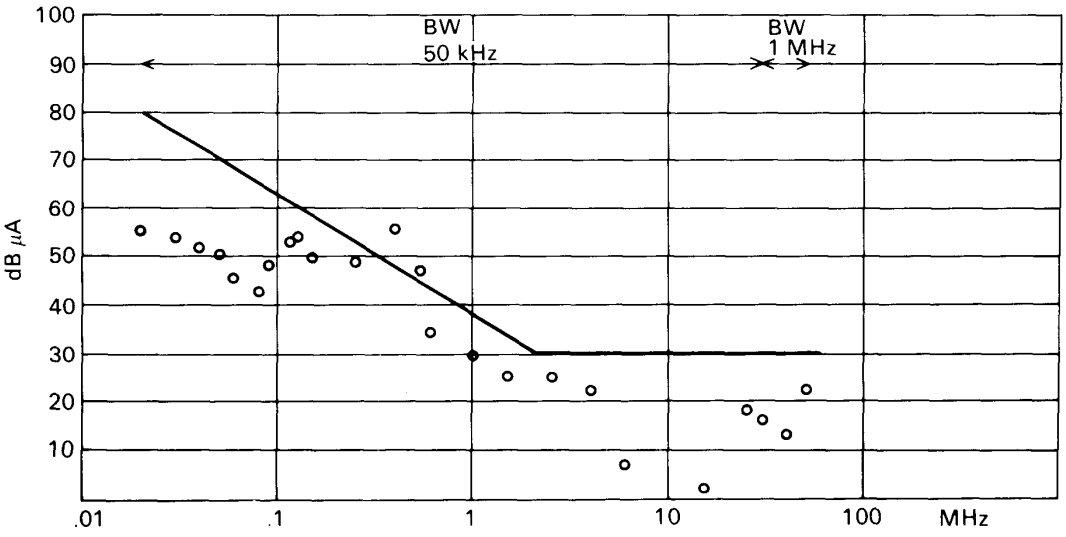

FIG. 3–9. EBA CE03 DH (NB) Fire 5 kV 630 mA 0.5 s.

Fig. 3–9, respectively. In these figures, DH means differential hot. Noises are well controlled.

(4) MPD CE (Power Line)

Data obtained are shown in Fig. 3–10 for dummy load mode and Fig. 3–11 for firing mode. Over spec. points appear on 28V PWR Power line for both dummy and firing modes. The line is separated and charger is turned off when MPD is firing. Therefore, noise is considered to be induced electromagnetically. Especially, at MPD firing, noise is seriously high. In order to minimize interferance to Spacelab power system, some immediate countermeasure must be taken.

(5) EBA/MPD RE (Magnetic Field)

Measurement of RE 04 was made for EBA and MPD firing. But background level were above the specification (60 dB_{pT}), and measurement was failed.

(6) EBA-MPD joint operation RE (Electric Field)

Test results are shown in Fig. 3–12. Although MPD was operated at nominal value,

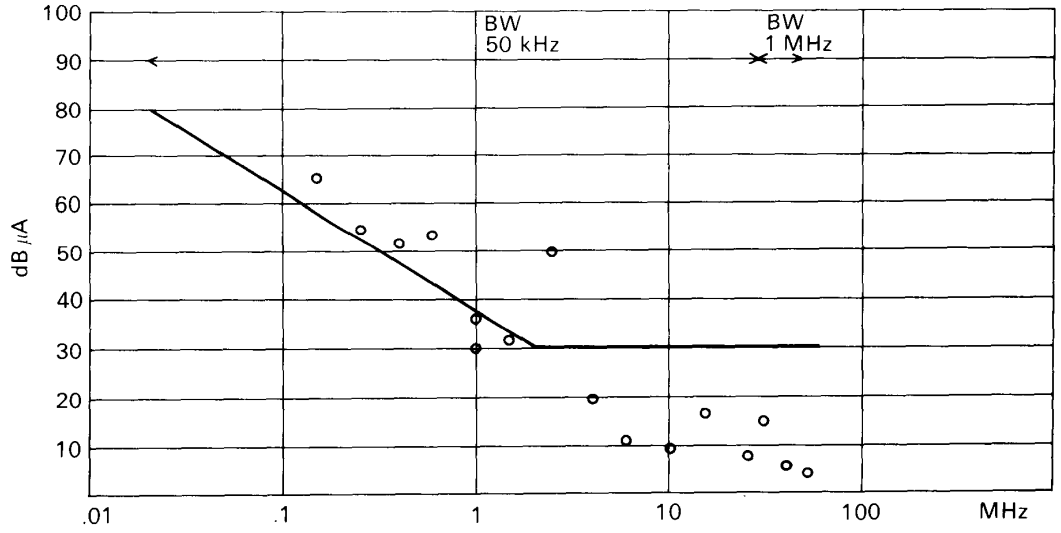

FIG. 3–10. MPD CE03 DH (NB) Dummy 480 V.

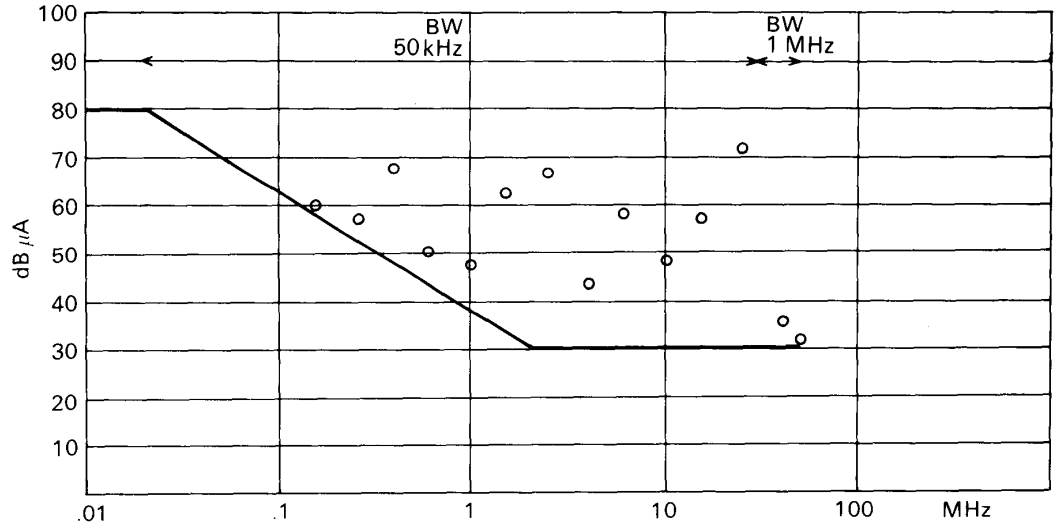

FIG. 3–11. MPD CE03 DH (NB) Fire 480 V 3 ATM.

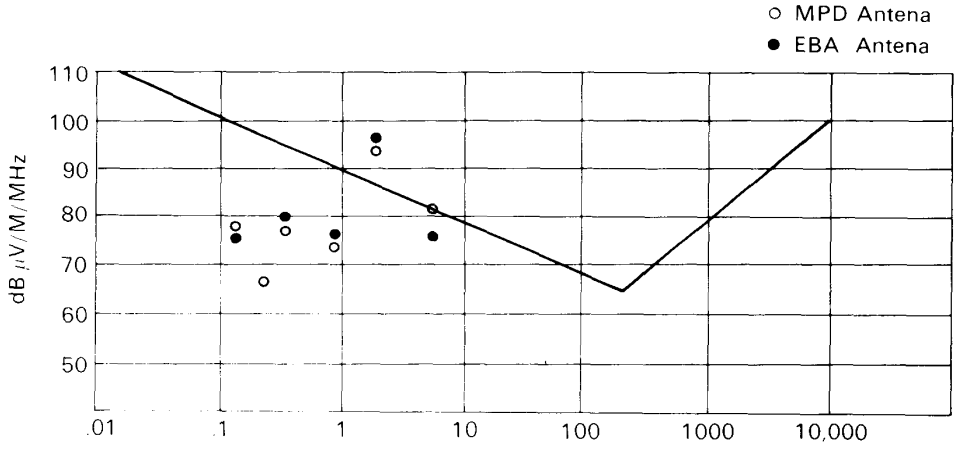

FIG. 3-12. EBA/MPD Joint Operation RE02 (BB). EBA 1 kV 60 mA, MPD 480 V 3 ATM.

EBA ejected only 1 kV beam under Configuration I. Data are calibrated for both EBA antenna factor and MPD one. As EBA power is extremely small, clear comments are not possible.

(7) RE measurement at critical frequencies

When MPD is firing, considerable noise is observed. Therefore, we must investigate whether there are influences of MPD noise for shuttle orbiter's communication system. Table 3-3 shows the data obtained for MPD firing at critical frequencies. For S band, data can be regarded as broad band and satisfy the specification. But for UHF band, data are scattered and even narrow band noises may be contained. Although MPD firing lasts only 1 msec and communication system may be disturbed a little, more detailed analysis will be required for UHF band. As far as EBA firing at critical frequencies is concerned, all data are broad band noise and below the specification.

TABLE 3-3. Noise measurement at critical frequencies

Band	Frequency (MHz)	Spec. (dB μV/m/MHz)	Measurement (dB μV/m/MHz)
UHF	259.7	67	62-80
	279.0	67	58-78
	296.8	67	67-92
S	2106.4	70	Below 40

(8) Functional verification of SEPAC system including DEP and IU under plasma environment was successfully confirmed.

4. ELECTRON BEAM SPREAD

The beam spread is one of the important criteria for the safety of this kind of electron beam experiments on the shuttle. The beam spread was measured by the

following instruments:

i) Current probe array (CPA)
ii) TRW Faraday cup
iii) TV camera
iv) Photometer

When the electron beam was emitted in the ground mode, the beam profile was clearly measured by those instruments listed above. In the floating mode experiment, the pallet potential rose to the level of the beam energy and most of the beam electron returned to the pallet. Only those electrons in the high energy tail of the beam could reach the chamber wall. The current of those electrons times the resistance between the pallet and the chamber wall equals to the beam voltage. The beam spread was very broad in the floating mode and it was very difficult to identify the beam profile. In the following, the results obtained by each instrument are described.

4.1 Ground Mode Experiment

4.1.1 Current probe array

The current probe array was located at the ceiling of the large chamber (9.5 m from the gun) and its layout is shown in Fig. 4–1. It was composed of 15 current probes.

In Fig. 4–1, a typical beam profile constructed from CPA data is shown for 1 kV 44 mA. From the measured current distribution the center of the beam spread and its FWHM radius are obtained. The distribution was obtained by assuming a proper profile with its peak value, center location, and FWHM as parameters. Since the total current and the values measured by the current probe array are known the best fit distribution was obtained. A typical change of the beam spread as a function of the focusing current is shown in Fig. 4–2 (A)–(E). When the focusing coil was not used, the beam would spread much, for example, it would spread to a radius of 5 m for a beam of 3 kV 300 mA (Fig. 4–3). The beam is really focused as shown in Fig. 4–2 by the focusing coil. However, the space charge effect of the beam of its own is fairly large and the minimum radius of the beam spread is 1.6 m. This means that the maximum power density of the beam deposited on the CPA is 0.15 kW/cm^3. Extrapolating this value to

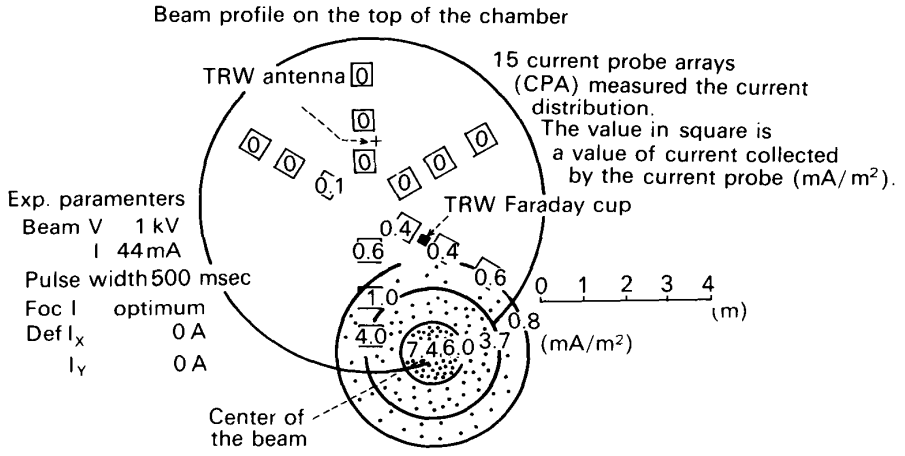

FIG. 4–1. Current probe array and beam profile in the top of the chamber.

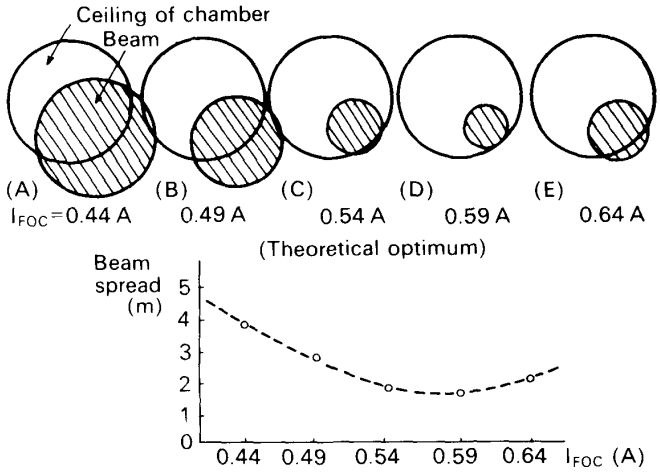

FIG. 4–2. Beam focusing pattern.

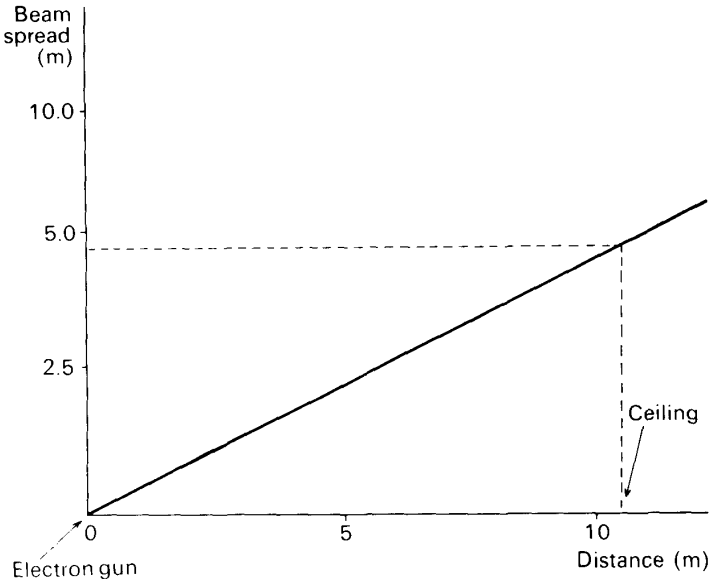

FIG. 4–3. Beam spread due to its own space charge.

the maximum power of SEPAC electron gun, the beam power density deposited on a surface at a distance of 10 m from the gun will be 1.5 kW/cm^3. About 200 shots of 0.5 to 1 sec pulsed beam were fired, but no damage nor any symptom of damage was detected on the CPA. From these data, it can be said that so long as the back ground pressure is below 10^{-6} Torr, the beam does not focus to a very thin beam due to its own space charge and has not enough power density to cause any damage on the surface where the electron beam is deposited.

4.1.2 TRW Faraday Cup

The beam spread measurement by the TRW Faraday cup was done by changing the deflection coil current and data are shown in Fig. 4–4. It agrees well with that obtained by the CPA.

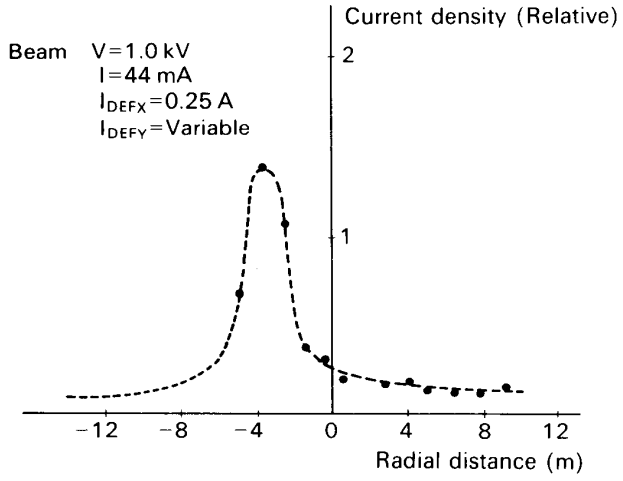

FIG. 4–4. Beam distribution on the ceiling of the chamber measured by TRW Faraday cup.

4.1.3 TV

Electron beam was emitted almost parallel to the magnetic field by using the deflection coil assembly. Approximately parallel beam was obtained when an adequate current was applied to the focusing coil, as shown in Fig. 4–5. Analyzing the pictures obtained by MTV, the beam spread in radial direction is found to be below 10 cm near the EBA exit and no interference with surrounding apparatus is observed. Emission spot excited by the beam attack at the chamber ceiling indicates that the electron beam expands about 1.5 m^{ϕ} in travelling 10 m (Fig. 4–6).

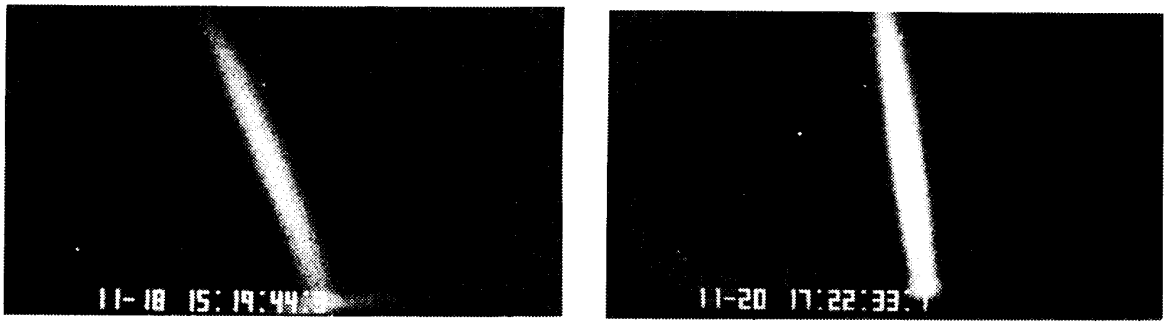

3 kV 0.26 A 7.5 kV 1.6 A

FIG. 4–5. Electron beam observed by MTV in the ground mode.

3 kV 0.26 A

FIG. 4–6. Beam spot on the ceiling observed by MTV.

4.2 Floating Mode Experiment

4.2.1 CPA and TRW Faraday Cup

In the floating mode experiment, no beam was detected by CPA and TRW Faraday cup. Only signal detected is due to a plasma which was produced by the ionization of outgas from the surface of the pallet-mounted instruments and mockup (Mockup models were mounted on the pallet to simulate SL-1 configuration).

4.2.2 TV

When EBA is operated in floating mode, equivalent amount of electrons to the beam

5 kV 0.6 A

FIG. 4–7. Electron beam observed by MTV in the floating mode.

(a) 5 kV 0.6 A before NGP operation (floating voltage = 5 kV)

(b) during NGP operation (floating voltage = 0)

(c) after NGP operation (floating voltage = 5 kV)

FIG. 4–8. Electron beam observed by MTV in EBA/NGP joint experiment.

current is supplied to the floating system (return current). The floating system is strongly illuminated by the bombardment of the return electrons. So the emission from the ejected beam gets relatively faint on the TV screen. The beam spread in floating mode operation is much larger than that in ground mode operation (Fig. 4–7), affected by the strong electric field between the chamber wall and the floating portion. The electron beam spreads out within 3 m and gets invisible.

MPD and NGP are used to reduce the charging effect. When either plasma plume or neutral gas plume is ejected in EBA floating mode operation, the charging of the system is completely neutralized, and beam spread remarkably changes according to the change of the charging voltage. This is shown in Fig. 4–8. The beam spread when the system is completely neturalized is similar to that in ground mode operation.

4.3 Discussion

In SEPAC experiment, the safety against the beam impingement on the shuttle surface is assured in the following ways:

(i) The experiment is planned in advance in such a way that the beam trajectory never hits the shuttle surface.

(ii) A software mask program is prepared in the SL-1 Experiment Computer (EC) to inhibit the beam emission when there is a possibility that the beam will hit the shuttle surface.

(iii) The beam spread is measured in laboratory experiment to assure that the damage on the shuttle surface is negligible even if the beam hits the shuttle surface. The beam spread measured in laboratory experiments will be taken into account in the software mask design in (ii).

In this experiment, especially in Floating mode experiment, most of the electrons emitted from the electron gun return and hit the surface of the pallet-mounted instruments. It was feared that the surface would be damaged. Neither significant damage nor its symptoms are detected at all on the surface of thermal blankets and other metal and insulator surfaces of the pallet-mounted instruments and mockups.

Another fear was that the beam would hit the shuttle surface when either the shuttle attitude, the magnetic field calculation or the deflection coil does not work normally. As discussed in 4.1.1, this experiment shows that the beam will spread due to its own space charge effect and the power density deposited on the surface will be insufficient to cause any damage. One extremely safe criterion is that the shuttle surface shall be less than that of the solar radiation. It corresponds to the beam radial spread of 1.5 m for 7.5 kV, 1.6 A beam. In a series of TV photographs taken in this experiment, the beam spread is much larger than this at a distance of 10 m. The beam spread is expected to depend strongly on the vacuum pressure. So long as the vacuum pressure around the shuttle is not higher than 10^{-5} Torr, the beam spread is will be fairly large so that the safety will be assured against the beam impingement.

5. Return Current Collection by Wire-Meshed Beta Cloth

5.1 Background of the Experiment

When an electron beam is emitted into space from shuttle, the orbiter will be

positively charged and space electrons will be collected through the orbiter conductive surface (return current). The amount of the return current depends on the conductive surface area of the shuttle, but the surface of the shuttle is mostly covered with non-conductive materials except its main engine portion. Spacelab module and payload instruments on pallet are covered with Beta cloth for thermal insulation. There is an argument that wire-meshed Beta cloth may be useful for the return current collection without sacrifice of the thermal insulation capability.

5.2 Objectives

This experiment is to investigate the return current collection capability of wire-meshed Beta cloth in a large chamber, when the electron beam is emitted in the floating mode.

5.3 Experimental Arrangement

Two types of return current collector were used as shown in Fig. 5–1. Type A is a 90 cm × 120 cm aluminum plate completely covered by wire meshed Beta cloth. Return current can only be collected by the mesh over the β-cloth. Type B is an aluminum plate of the same size and sus wire mesh is over the aluminum plate. Both meshes are composed of sus wire of the same size as 0.2 mm in diameter. Two collectors of each type were set in the chamber side by side in such a way as shown in Fig. 5–2 with a mutual separation of 17 ~ 50 cm. The currents into meshed wire of Beta cloth, meshed wire over the aluminum plate and the aluminum plate were measured separately. The static potential of the Beta cloth was not measured directly, but the charge probe brought from Utah State University was set nearby so that the potential information can be obtained from it.

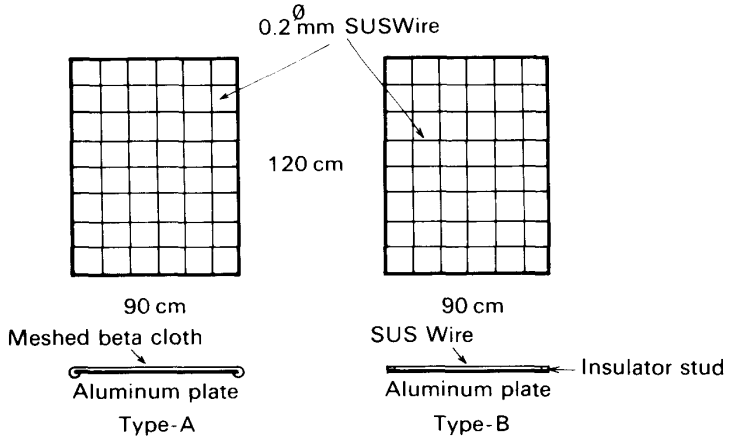

FIG. 5–1. Return current collectors.

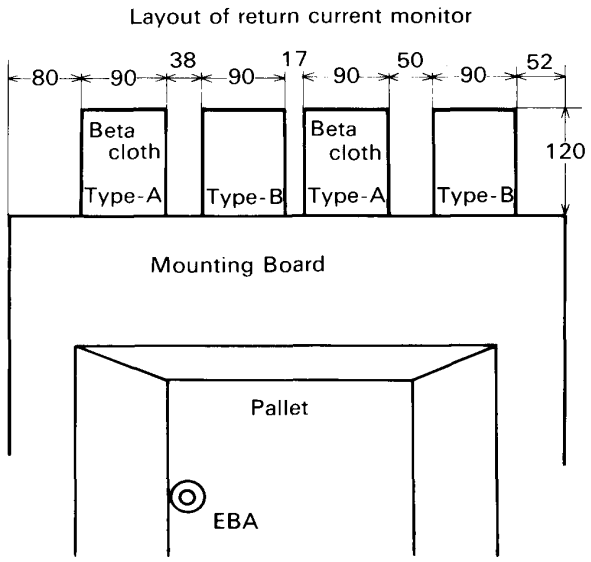

FIG. 5–2. Arrangement of return current collectors in the chamber.

5.4 *Experimental Results*

The experiment was done in Configuration II and I, but in Configuration II, the isolation between the meshed-wire and the common ground was not enough so that no meaningful data was obtained. In Configuration I, data was taken in both floating mode and MPD/EBA joint experiment mode. The results are shown in Fig. 5–3 (a) and (b). The quantity of data is limited because of very limited time for Configuration I. In Fig. 5–3, the wave form of the pallet potential is shown together with those for currents into the wire-meshes and the aluminum plate. The numbers in percent in parethesis shows the percentage ratio of the current into either the mesh on the Beta cloth or the mesh over the plate to that into the aluminum plate. The results are summarized in Table 5–1. As can be seen from these data, the wire mesh over the aluminum plate collects a few % of that collected by the aluminum plate. This is much higher than the ratio of surface area (500 : 1). The wire mesh over the Beta cloth collects much more and it amounts to more than 10%.

The reason why the wire mesh can collect more than its surface area can be understood in the following way:

The return current electrons have nearly the same energy as the beam electrons. They impinge on the surface as shown in Fig. 5–4 and an outgas cloud is formed near the surface. The return current electrons ionize it and create plasma. Electrons in the created plasma flow into the meshed wire together with the primary return electrons. Around the meshed wire, a sheath is formed and all thermal electrons flowing into the sheath edge are collected by the wire. In other words, the effective surface area of the wire increases when a plasma is created around it. The plasma density created is supposed to be around $10^6/cm^3$. Whether the difference between the current collected

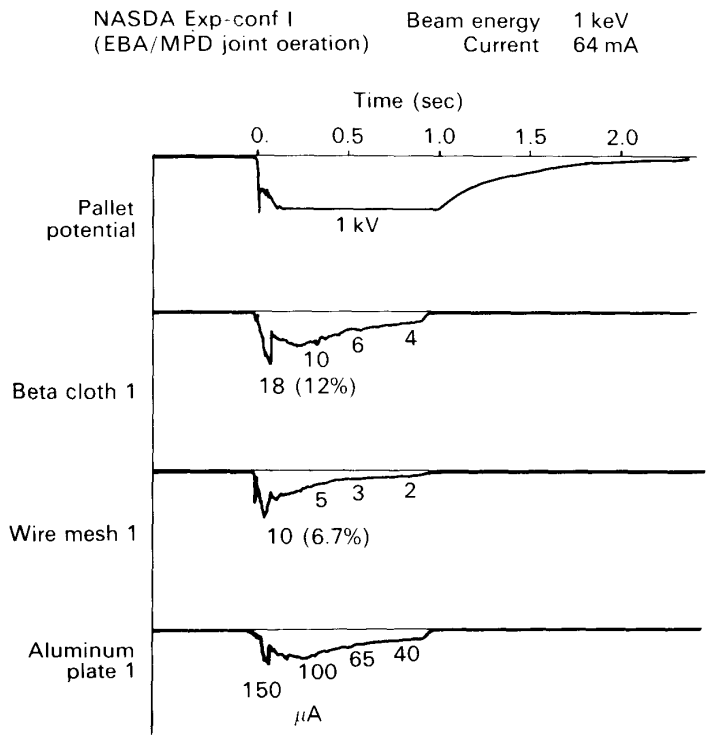

FIG. 5–3 (a). Return current collection by wire-meshed Beta cloth and wire-mesh over Aluminum plate. EBA floating mode.

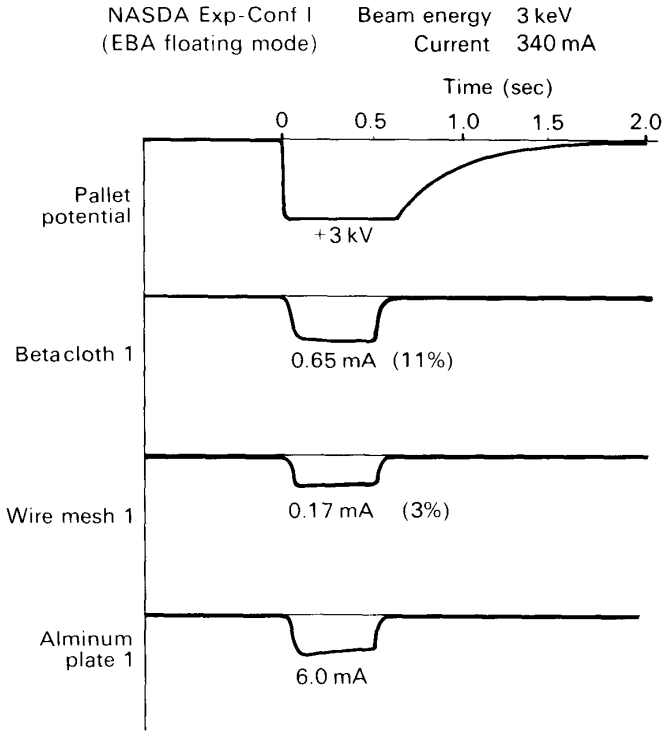

FIG. 5–3 (b). Return current collection by wire-meshed Beta cloth and wire-mesh over Aluminum plate. EBA/MPD joint experiment mode.

TABLE 5–1. List of currents collected by β-clothes and mesh over metal plate

Electron beam	β-Cloth 1	Mesh over Metal plate 1	Metal plate 1	β-Cloth 2	Mesh over Metal plate 2	Metal plate 2
3 kV 300 mA	0.65 mA (11%)	0.17 mA (3%)	6.0 mA	0.51 mA (7.5%)	0.30 mA (4.3%)	7.0 mA
1 kV 64 mA	20 μA (14%)	14 μA (10%)	140 μA	50 μA (25%)	16 μA (8%)	200 μA

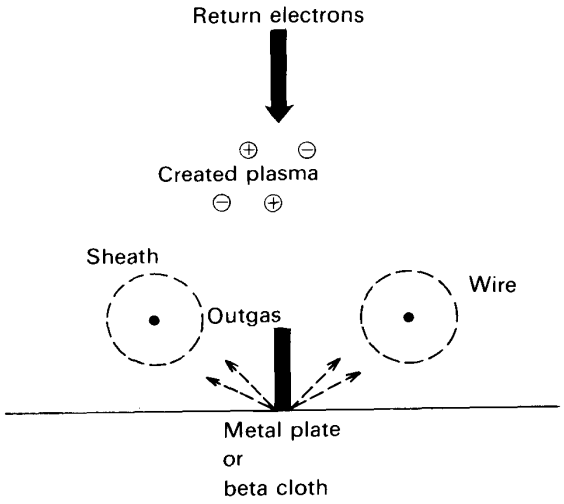

FIG. 5–4. Mechanism of return current collection by mesh over β-cloth/metal plate.

by the meshed wire on the Beta cloth and that by the meshed wire over the metal plate is meaningful cannot be concluded in this experiment, but at least it is concluded that the wire-meshed Beta cloth can collect a return current with an effective area of about 10%.

6. MPD ARCJET CONTAMINATION EFFECT

The discharge circuit of the MPD arcjet is isolated from the shuttle ground so that the current path may not be formed through the supporting structures and neighboring instruments. It has been feared, however, that discharge spots, i.e. sputtering, would be formed on the metal surface in abnormal operating conditions where the mass flow rate of argon gas is insufficient. It is checked by cleanly polished metal surface whether the arc discharge sputters the neighboring surface as well as whether the plasma contaminates the surface during normal 100 shots of MPD arcjet.

The construction of the contamination monitor is shown in Fig. 6–1. Four pieces of metal plate are mounted in the monitor box. Two of them, #1 or 5 and #3 or 7, are hidden behind the front panel. The centers of the two plates, #2 or 6 and #4 or 8, are aligned with those of circular windows opened in the front panel. A metal blade, which can rotate around the center axis of the front panel, shuts off the windows while the monitor is not working. These two plates are exposed to the chamber environment only

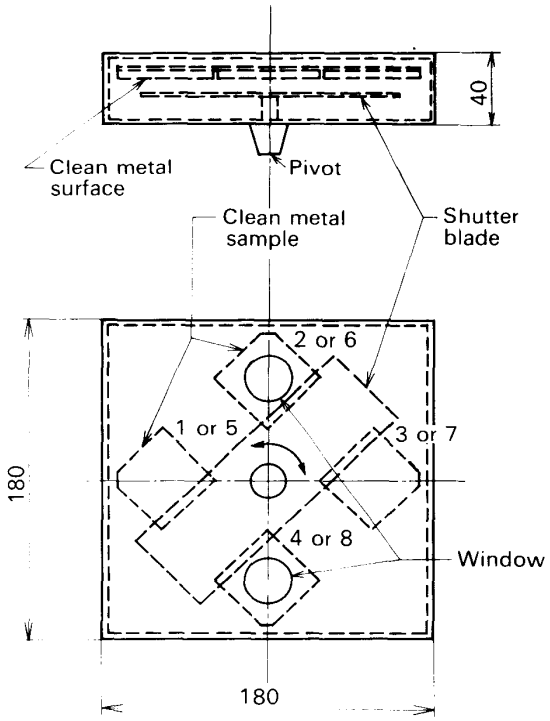

FIG. 6–1. Contamination monitor. Dimensions are expressed in millimeter.

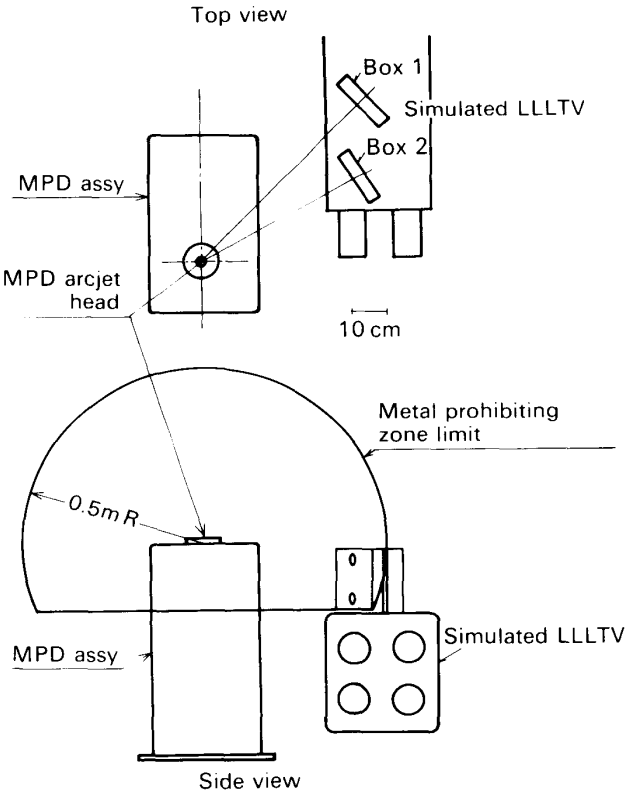

FIG. 6–2. Monitoring box arrangement.

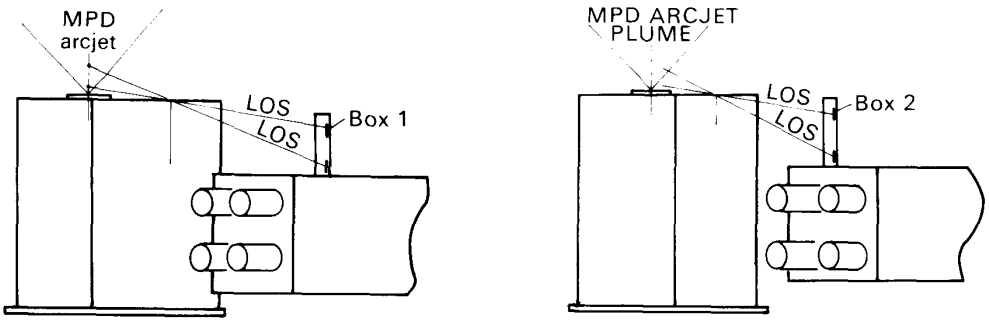

FIG. 6–3. LOS for highest incident angle of plasma particle impingement (Box 1 and Box 2).

when the 100 shots are made. If the roughness of the hidden and exposed surfaces are compared after the test, the net effect of sputtering and plasma contamination is determined. Two sets of the contamination monitor are placed at the top of the Low Light Level TV (INS 003) as shown in Figs. 6–2, 6–3 and 6–4.

The roughness of the polished metal surface was measured by a roughness meter Tokyo Seimitsu SURFCOM E-RM-30A before and after the test. The tracing regions of the roughness measurement are indicated in Fig. 6–5. A single Y-trace was made before the test and an X- and a Y-traces were made after the test. The recorded traces are illustrated in Fig. 6–6. The maximum roughness height of each plate was measured

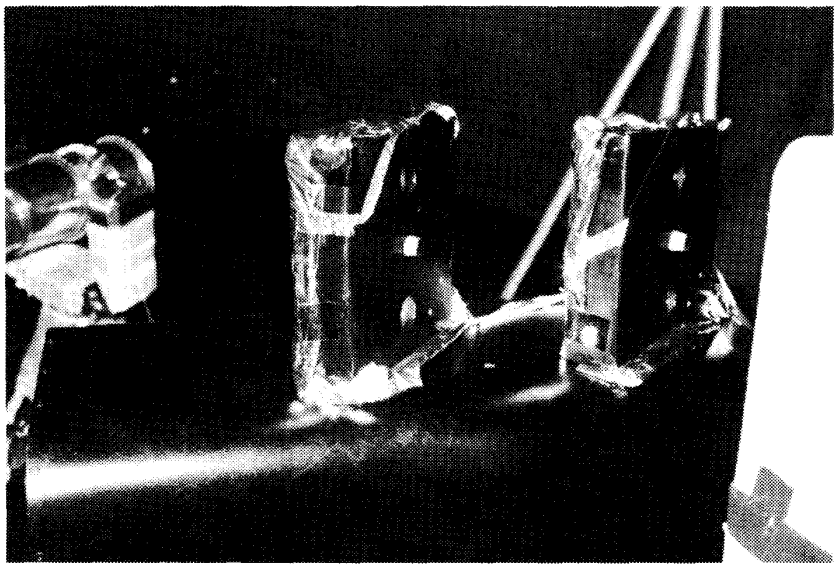

FIG. 6–4. Contamination monitor mounted on LLLTV (INS003).

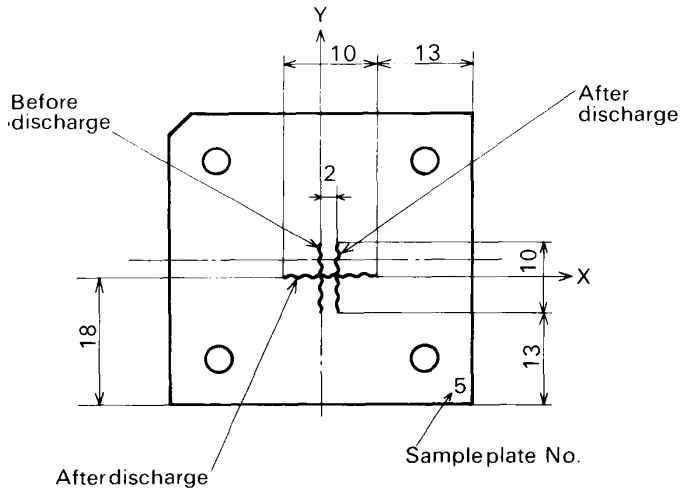

FIG. 6–5. Sampling trace on metal surface for roughness measurement.

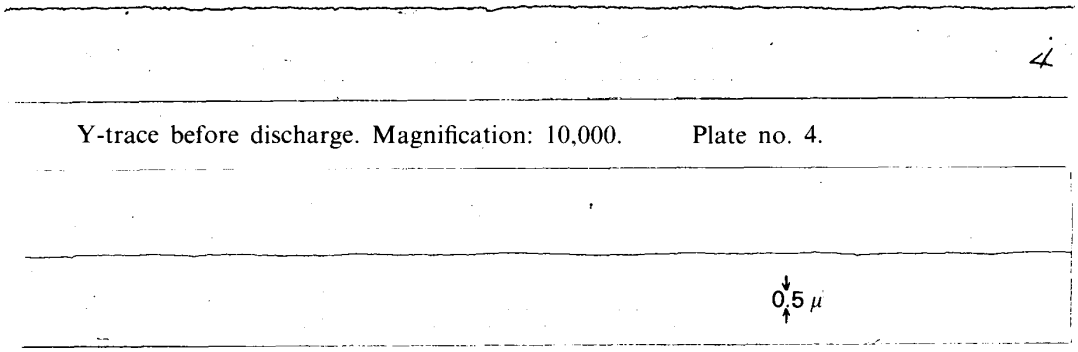

Y-trace before discharge. Magnification: 10,000. Plate no. 4.

Y-trace after discharge. Magnification: 10,000. Plate no. 4.

FIG. 6–6. Roughness tracing of contamination measurement.

TABLE 6-1. Maximum roughness height sampled on the metal plate

Metal plate	Before discharge	After discharge	
	Y-trace (μm)	X-trace (μm)	Y-trace (μm)
#1	0.10	0.20	0.15
#2	0.25	0.10	0.25
#3	0.25	0.20	0.20
#4	0.10	0.20	0.10
#5	0.30	0.15	0.25
#6	0.25	0.10	0.20
#7	0.30	0.15	0.20
#8	0.30	0.10	0.20

and listed in Table 6-1. No significant change due to sputtering as well as due to contamination was found in the data obtained before and after the test. The eye inspection over the entire surface of each sampling plate confirmed no change in the surface conditions.

7. LIGHT EMISSION MEASUREMENT OF MPD PLASMA BY PHO

The PHO (Photometer) monitors the irradiance in the visible region due to interactions of electron beams from EBA and plasma beam from MPD with a neutral gas. Among various emission lines which are expected in the experiment, N_2^+ (3914 Å), O (5577 Å and 6300 Å) are selected. The field of view is determined by iris from 9 to dark (in 16 steps), and by optical axis which is controlled by the gimbal system, i.e., zenith $-60°$ to 64 (in 32 steps).

The light emission from MPD plasma flow was observed by PHO. The viewing angle was varied by the gimbal mechanism. The location of the plasma stream aimed at by the PHO is illustrared in Fig. 7-1. The half-value radius of the plasma density is also

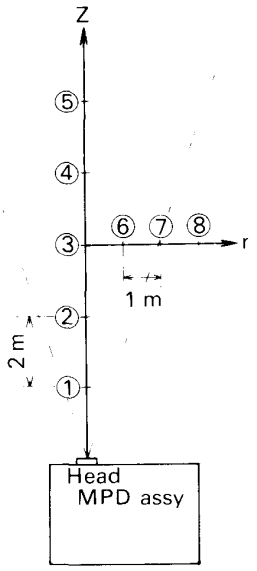

FIG. 7-1. PHO observation point of MPD plasma plume.

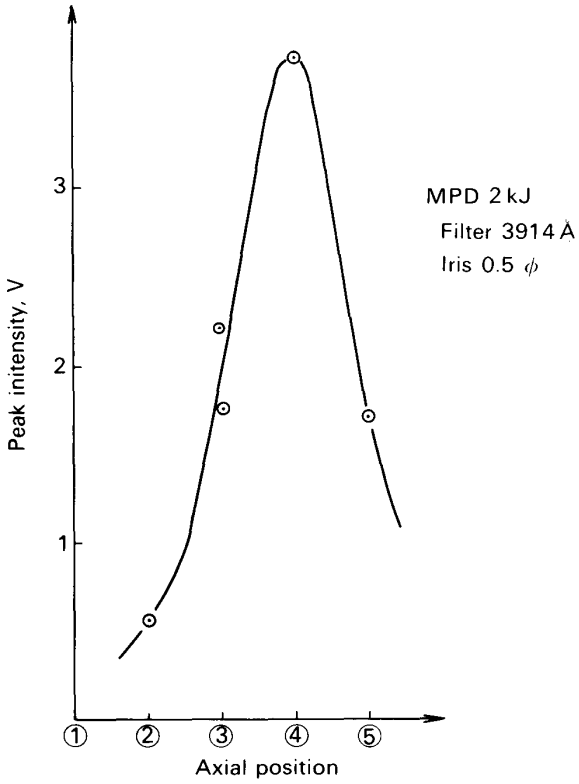

FIG. 7–2. Peak intensity distribution on 3914 Å emission.

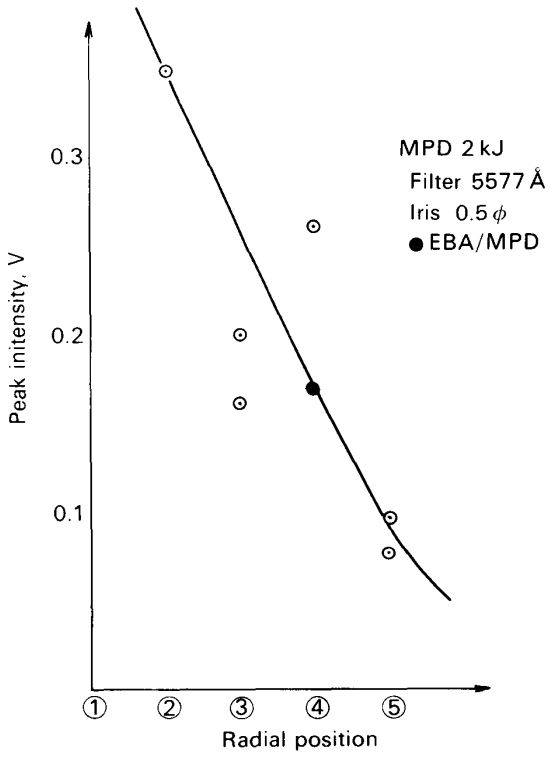

FIG. 7–3. Peak intensity distribution of 5577 Å emission.

expressed by broken lines in Fig. 7–1.

The streamwise variation of light intensity are shown in Figs. 7–2 and 7–3. The contrast between the distributions for 3914 Å and 5577 Å is remarkable. The profile for 3914 Å has a sharp peak at the location 4, while that for 5577 Å shows a decreasing function from jet exit towards downstream. The monotonous decrease simply results from the plasma expansion and the loss of exciting agent. No plausible explanation has yet been given for this difference. If the peak in the 3914 Å intensity distribution is due

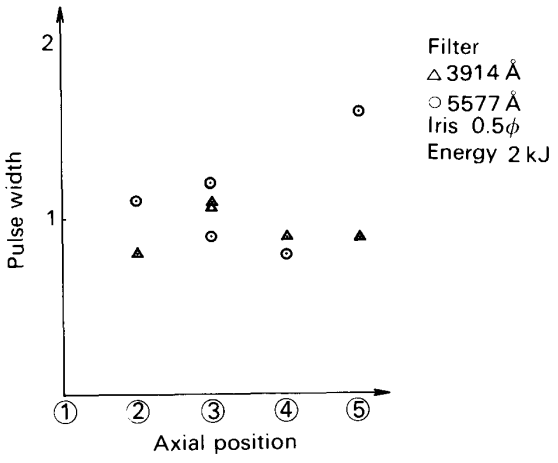

FIG. 7–4. Pulse width of light pulse.

to the chamber wall reflection, the same feature should appear in other distributions. Although the oxygen atom does not exist in the space chamber atmosphere, the argon plasma is dense and energetic enough to dissociate the oxygen molecules. The bremsstrahlung which originates from the argon plasma was estimated. The intensity calculated for the bremsstrahlung was much less than those for N_2^+ and O emissions.

The pulse width of the light emission is plotted in Fig. 7–4. The widths of both 3914 Å and 5577 Å radiation pulse are both about 1 msec. If we consider the N_2 and O_2 molecules are immobile and the plasma particles pass by them, the pulse width is determined by either plasma duration or the lifetime of the excited states. Since the excited states of N_2 is short-lived, the pulse width comparable to the plasma duration is reasonable. The excited state of $O(^1S)$, on the other hand, has a life time of 1.4 sec. Hence, the pulse width of 5577 Å radiation is too short to be attributed to the O excitation. As mentioned earlier, the contribution from the bremsstrahlung has been estimated to be negligible.

8. ISAS Test Participants

The member of ISAS team participated in this experiment is listed below.

o General Test Conductor	T. Obayashi
o Test Manager	K. Kuriki M. Nagatomo
o Electron Beam Acclerator	N. Kawashima I. Kudo A. Yamori Toshiba Elec. Co.
o MPD Arcjet/Neutral Gas Plume	K. Kuriki Y. Shimizu Mitsubishi Elec. Co. Meisei Elec. Co. Mitsubishi Heavy Ind.
o Diagnostic Probe	M. Ejiri S. Miyatake I. Nagano Nippon Elec. Co. Meisei Elec. Co.
o Monitor TV	S. Sasaki Toshiba Elec. Co.
o CD Support	K. Ninomiya A. Onishi Nippon Elec. Co.
o EMI Test	I. Kudo Mitsubishi Elec. Co.

o Mechanical Structure	T. Araki Ushio Elec. Co. Yushiya Man. Co.

9. SUMMARY

SEPAC Proto Models were successfully operated in the NASDA Space Chamber. The test results are

1) Correlation between PFP and spacecraft potentials was obtained,
2) EMI data were obtained for EBA and MPD firing,
3) EBA beam spread was measured for the software mask design,
4) Capability of wire-meshed beta cloth as reutrn currrent collector was evaluated,
5) Effect of MPD arcjet firing on the surrounding equipment was measured.

Institute of Space and Aeronautical Science
University of Tokyo
September 8, 1979

REFERENCES

[1] T. Obayashi, K. Kuriki, N. Kawashima, M. Nagatomo, I. Kudo, K. Ninomiya, A. Ushirokawa, M. Ejiri, and S. Sasaki, ISAS Report No. 562, 1978.
[2] D. B. Beard and F. S. Johnson, *J. Geophys. Res.*, **66** (1961) 4113.